Robust Bidding Strategy for Multi-energy Virtual Power Plant in Peak-regulation Ancillary Service Market Considering Uncertainties

Yong Li[1], Youyue Deng[1], Yahui Wang[1], Lin Jiang[2], and Mohammad Shahidehpour[3]

[1] College of Electrical and Information Engineering, Hunan University, Changsha, China

[2] Department of Electrical Engineering and Electronics, University of Liverpool, Liverpool, UK

[3] Galvin Center for Electricity Innovation, Illinois Institute of Technology, Chicago, USA

***Abstract*—Multi-energy virtual power plant (MEVPP) can aggregate flexible resources such as energy storage and flexible loads that decentralized in the region to meet the access conditions in the peak-regulation ancillary service market. However, the uncertainties in energy sources and loads bring adverse impact on the operation of MEVPP. Therefore, this paper proposes a day-ahead robust bidding strategy for MEVPP to participate in the peak-regulation market. Firstly, this paper analyzes the impact of uncertainties for MEVPP on the peak-regulation market. On this basis, the operation mechanism for MEVPP in the peak-regulation market is proposed by considering the integrated demand response (IDR). Additionally, the day-ahead two-stage robust bidding model is established to minimize the operation cost of MEVPP. Finally, the case studies show that the day-ahead robust bidding strategy can effectively reduce the peak-regulation deviation penalty compared with traditional deterministic optimization. Specifically, with the proposed robust bidding strategy, the total revenue in the actual operation stage is increased by 5.16% and 8.45% on sunny day and raised by 8.28% and 15.35% on cloudy day when the predicted deviations are respectively 20% and 30%, comparing with traditional deterministic optimization.**

***Index Terms*-- Uncertainty, multi-energy virtual power plant, robust bidding strategy, peak-regulation market**

NOMENCLATURE

Abbreviations

VPP	Virtual power plant	DERs	Distributed energy resources
		ESSs	Energy storage systems

CVaR	Conditional value at risk
PV	Photovoltaic units
IES	Integrated energy system
MEVPP	Multi-energy virtual power plant
IDR	Integrated demand responds
MEVPPO	Multi-energy virtual power plant operator
CCHP	Combined cooling, heat and power cogeneration unit
C&CG	Column-and-constraint generation algorithm

Indices and sets

t	Index of time interval (h)
l	Set of energy storage devices
T_{p} / T_{v}	Set of peak and valley periods (h)

Parameters

$P_{\mathrm{tr}}^{\max}$	Upper limit of power of transferred electrical load (kW)
$T_{\mathrm{hw}}^{\min}$ / $T_{\mathrm{hw}}^{\max}$ / T_{hw}^{0}	Minimum/maximum/initial water temperature (°C)
c_{w}	Specific heat capacity of water (kWh/(kg·°C))
ρ_{w}	Density of water (kg/m^3)
$T_{\mathrm{in}}^{\max}$ / $T_{\mathrm{in}}^{\min}$	Maximum/minimum indoor temperature (°C)
R	Thermal resistance of the house (°C/kW)
$P_{\mathrm{GT}}^{\mathrm{N}}$	Rated capacity of natural gas to electricity by gas turbine (kW)
$\eta_{\mathrm{GT}}^{\mathrm{e}}$	Conversion efficiency of natural gas to electricity by gas turbine
$\eta_{\mathrm{LB}}^{\mathrm{h}}$ / $\eta_{\mathrm{LB}}^{\mathrm{c}}$	Conversion efficiency of the waste heat of flue gas to thermal/cooling energy by lithium bromide unit
$\eta_{\mathrm{GT}}^{\mathrm{h}}$	Conversion efficiency of natural gas to the waste heat of flue gas by gas turbine
$H_{\mathrm{LB}}^{\mathrm{N}}$ / $C_{\mathrm{LB}}^{\mathrm{N}}$	Rated thermal/cooling output by lithium bromide unit (kW)
COP_{HP}	Coefficient of performance of heat pump
$H_{\mathrm{HP}}^{\mathrm{N}}$	Rated output of heat pump (kW)
COP_{cen}	Coefficient of performance of centrifugal chiller
$C_{\mathrm{cen}}^{\mathrm{N}}$	Rated output of centrifugal chiller (kW)
α_l	Energy loss of energy storage devices
η_l^{c} / η_l^{d}	Charging/discharging efficiencies
$SoC_l^{\min}$ / $SoC_l^{\max}$	Minimum/maximum state of charge
S_l^{N}	Rated energy storage capacity (kWh)
$P_l^{\max}$	Maximum charging and discharging power (kW)
n_{room}	Number of rooms
P_{base}^t	Baseline power purchased from the grid (kW)
$P_{\mathrm{f,min}}^t$	Lower bound of the bidding power (kW)
$P_{\mathrm{p}}^{\max}$ / $P_{\mathrm{v}}^{\max}$	Upper bounds of the bidding power (kW)
ς_{gas}	Calorific value of natural gas (kJ/m^3)
c_{gas}^t	Price of natural gas (RMB/m^3)
c_{grid}^t	Price of electricity from the grid (RMB/kWh)
c_l	Operation cost coefficient of the energy storage (RMB/kWh)
c_{tr}^t	Compensation price to regulate electrical loads (RMB/kWh)
c_{sc}^t / c_{sh}^t / c_{se}^t	Price of cooling/thermal/electrical energy (RMB/kWh)
c_{p}^t / c_{v}^t	Prices for peak shaving and valley filling in the peak-regulation market (RMB/kWh)

Variables

P_{eload}^t	Power of the electrical load after optimization (kW)
P_{tr}^t	Power of the transferred electrical load (kW)
H_{hload}^t	Power of the thermal load (kW)
C_{cload}^t	Power of the cooling load (kW)
P_{GT}^t	Electrical energy generated by gas turbine (kW)
H_{LB}^t / C_{LB}^t	Thermal and cooling energy generated by lithium bromide unit (kW)
H_{HP}^t	The thermal energy generated by heat pump (kW)
C_{cen}^t	Cooling energy generated by centrifugal chiller (kW)
P_{cen}^t	Electricity consumed by centrifugal chiller (kW)
S_l^t	Energy storage level (kWh)
$P_{l,\mathrm{c}}^t$ / $P_{l,\mathrm{d}}^t$	Charging/discharging power (kW)
P_{p}^t / P_{v}^t	Bidding power of peak shaving and valley filling (kW)
P_{grid}^t	Electrical power purchased from the grid (kW)
u_{ed}^t / u_{cw}^t / u_{out}^t / u_{pv}^t	Uncertainty values of the initial electrical load (kW), the volume of cold water (L), the outdoor temperature (°C) and the power output of PV (kW)

x_{LB}^t / x_{p}^t / x_{v}^t	Binary variables	P_{edu}^t / V_{cwu}^t / T_{outu}^t / P_{pvu}^t	The initial electrical load (kW), the volume of cold water (L), the outdoor temperature (°C) and the power output of PV (kW)

1. Introduction

Generally, the capacity of decentralized distributed energy resources (DERs) is too small to meet the access conditions of energy market. Virtual power plant (VPP) is an effective way to integrate flexible resources such as various DERs, energy storage systems (ESSs), and flexible loads together by using information and communication technology to participate in the energy market [1][2][3]. With the development of integrated energy system (IES), multi-energy virtual power plant (MEVPP) is emerged as a new concept [4][5][6]. Compared with traditional VPP, MEVPP integrates multiple types of energy, such as electricity, thermal energy, cooling energy, natural gas, etc., which makes it suitable to participate in the energy market [5]. Moreover, to coordinate multiple energy sources and improve energy efficiency, it is an irresistible trend that traditional demand response transforms to integrated demand response (IDR).

In recent years, there are some documents dedicated to optimal dispatching of VPP. Reference [7] classifies different users and formulates different incentive prices by data mining, aiming to maximize the interests of users and minimize the operation cost of VPP. A multi-objective optimization model of power-to-gas based VPP is proposed in [8], maximizing profit and minimizing risk. However, the study considers the interaction between electrical energy and gas but does not consider cooling energy and thermal energy. In order to aggregate massive decentralized DERs and protect the privacy of the asset owners, literature [9] proposes a decentralized economic dispatch method and a decentralized VPP architecture, but the architecture only investigates pure electrical VPP. Some scholars turn their attention to MEVPP with multiple types of energies. Considering day-ahead profit maximization and emissions minimization, a multi-objective scheduling method of DERs in the MEVPP is proposed in literature [10]. Study [11] proposes a day-ahead optimal scheduling method for MEVPP, considering the multi-flexible performance of electric vehicle and the uncertainties of renewable energy resources at the generation side. However, works [10]-[11] only focus on optimal operations of MEVPP under the energy market, but do not take into account the bidding strategies of MEVPP in the peak-regulation ancillary service market. Thus, to further improve the economy of MEVPP, this

paper establishes a day-ahead bidding strategy for MEVPP to participate in peak-regulation market.

In China, with the increasing power demand of users, the power system peak load appears in winter and summer, and the peak-valley difference is constantly expanding. Thus, the pressure of peak-regulation of the grid increases continuously. MEVPP is a novel and flexible mode of peak-regulation, which can aggregate massive decentralized flexible resources. At present, the Chinese government has release relevant policies to encourage third party with energy storage devices and demand-side resources to participate in the provision of auxiliary power services [12]. In the future, the Chinese government will carry out demonstration projects on VPP, including industrial adjustable load, building air conditioning load, big data center load, energy storage, vehicle-to-grid (V2G) and other resources [13]. China aims to achieve a demand-side response capacity of 3%-5% of maximum load by 2025. Therefore, it is significant to design the bidding strategy for MEVPP in the peak-regulation market.

There are some researches about MEVPP participating in the peak-regulation market. For instance, based on reinforcement learning algorithm, a scheduling method for MEVPP participating in the peak-regulation market is proposed, and the response characteristics of DERs are analyzed [14]. Reference [15] combines traditional thermal power units with new VPPs and proposes a distributed double-layer clearing model under the peak-regulation market to improve the robustness against cyber-attacks. At the same time, the upper-level clearing model is proposed to ensure the fairness of power distribution among DER. Literature [16] designs the market mechanism for VPPs to participate in the deep peak regulation and establishes the day-ahead clearing model and the real-time clearing model for the thermal power units and VPPs. Finally, the case study is conducted to verify the effectiveness of the proposed mechanism. It also can effectively cope with the changes of real-time deep peak regulation demands. The above literatures discuss the market clearing model of MEVPP and the response characteristics of various equipment. However, they still have some limitations. Firstly, they do not consider the impact of the uncertainties within MEVPP on its participation in the peak-regulation market. In addition, the operation mechanism for a single MEVPP to participating in the peak-regulation market is not established.

To combat climate change, the Chinese government aims to peak carbon dioxide emissions by 2030 and become carbon neutral by 2060. To achieve this goal, the installed capacity of renewable energy resources in China is increasing. But renewable energy is volatile. It is a critical task for MEVPP to handle the uncertainties of renewable energy when participating in peak-regulation market. In addition, compared with pure electrical VPPs, MEVPP consists of different types of energy. Thus, MEVPP must deal with multiple uncertainties from sources such as PV,

electrical load, the volume of cold water, and the outdoor temperature. To solve this problem, stochastic optimization methods are widely used. To describe the uncertainty of VPP, literature [17] introduces the conditional value at risk (CVaR) and confidence method. For the joint market of energy and spinning reserve service, a two-stage stochastic programming method is used to establish a risk aversion model of VPP in [18]. The research in [19] establishes a double-layer scenario-based stochastic optimization model by using CVaR. Based on scenarios, the uncertainty of output of wind turbines and photovoltaic (PV) units is described, and a risk-constrained stochastic model of VPP is presented in [20]. The stochastic optimization method is relatively simple in calculation, which describes the uncertainty by scenario-based approaches. But it requires a lot of historical data to construct typical scenarios. Moreover, the computational burden will grow greatly with the increase of the number of scenarios, which makes it difficult to apply in practical engineering [21][22].

Compared with stochastic optimization, robust optimization does not require the specific probability distribution of uncertainty parameters, but only need obtain their bounded range, which is more suitable for MEVPP to formulate day-ahead bidding strategy in the peak-regulation market [23]. To solve the problem of uncertainties in renewable resource and imbalance penalty prices, a VPP robust bidding approach is proposed to maximize its profits in [22]. The research in [24] establishes a VPP robust optimization model to maximize benefits, in which the uncertainties of renewable energy sources and the demand response are incorporated. Authors of [25] use confidence bounds to present uncertainties in wind power and market prices and then put forward a two-stage optimization method based on robust optimization.

A day-ahead robust bidding strategy for MEVPP in the peak-regulation market is proposed in this paper, considering IDR and the uncertainties in source and load. The main highlights of this paper are as follows:

(1) The operation mechanism for MEVPP participating in the peak regulating market is established, which integrates various decentralized flexible resources in the region. (2) In view of the challenges brought by multiple uncertainties of renewable energy and various loads within MEVPP, a day-ahead robust bidding model is established to minimize the cost of MEVPP and improve the robustness of the system. (3) Apart from electricity, multiple forms of energy such as cooling energy, thermal energy, and natural gas are also involved in the peak-regulation market.

The rest of this article is organized as follows. Section 2 describes the operation mechanism for MEVPP. In Section 3, the mathematical model of MEVPP is presented. Section 4 gives the day-ahead robust bidding model. Validation and analysis are provided in Section 5. Finally, Section 6 concludes the article.

2. Operation mechanism for MEVPP

In the peak-regulation market, MEVPP coordinates IDR and ESSs to reduce electricity purchased from grid during peak periods and increase electricity input during valley periods. Thus, MEVPP obtains peak-regulation compensation through peak shaving and valley filling. Note that electricity is not considered to be sold to the grid in this paper.

The operation mechanism for MEVPP to participate in the peak-regulation market is shown in Fig. 1. To meet the access conditions of peak-regulation market, MEVPP integrates decentralized flexible resources in different energy forms, such as various DERs, ESSs, energy supply equipment, flexible electrical loads, flexible thermal loads, flexible cooling loads. In MEVPP, multi-energy virtual power plant operator (MEVPPO), as a manager, not only trades and bids with the external market, but also coordinates various internal resources to maintain the stability of the system. The process for MEVPP to participate in the peak-regulation market is as follows:

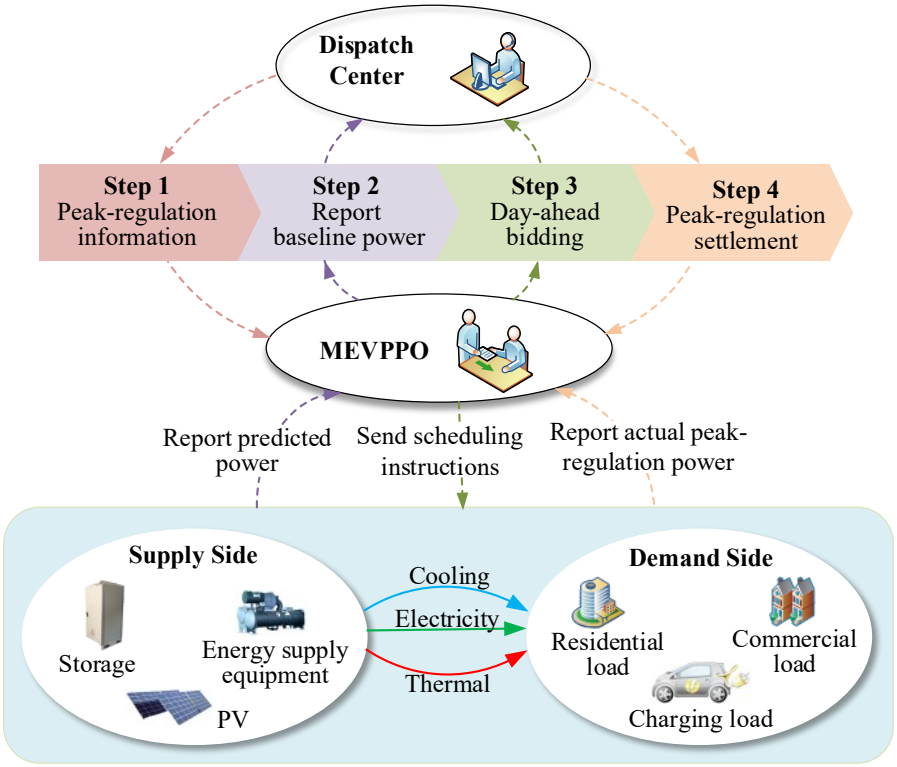

Fig. 1. Operation mechanism for MEVPP.

Step 1: Announce peak-regulation information. Before the operation day, the dispatch center announces peak-regulation information, such as prices, periods and access conditions.

Step 2: Report baseline power. Each aggregation unit in MEVPP reports information to MEVPPO according to day-ahead prediction results, including equipment capacity, load demands, periods, etc. Then, MEVPPO reports the baseline power of electricity purchased from the grid to the dispatch center. The baseline power is the net load of the

system based on the day-ahead prediction results. Notably, the uncertainties in source and load, and the effect of IDR and ESSs are not considered in this step.

Step 3: Day-ahead bidding. MEVPPO formulates a day-ahead bidding strategy based on the information sent by the internal participants and announced by the external peak-regulation market. Then, MEVPPO reports the peak-regulation bidding capacity and periods to the dispatch center.

Step 4: Peak-regulation settlement. After the operation day, the peak-regulation fee and penalty are settled. When the actual peak-regulation capacity is greater than the bidding capacity, the settlement is according to the bidding capacity. However, when it is less than 80% of the bidding capacity, MEVPP will be penalized. The penalty is calculated based on the unfinished part. In other cases, settlements are based on the actual peak-regulation capacity.

According to Fig. 1, the settlement is calculated based on the actual operation results. However, the actual power of renewable source and load is stochastic, which may cause the actual peak-regulation capacity to be lower than the day-ahead bidding capacity, i.e., MEVPP may be penalized. Hence, when MEVPP formulates the day-ahead bidding strategy to participate in the peak-regulation market, it is significant to consider the uncertainties in source and load.

3. Mathematical model of MEVPP

The system structure of MEVPP is shown in Fig.2, which is based on a multi-energy station in China. The system includes ESSs, flexible loads, combined cooling, heat and power cogeneration unit (CCHP), etc., which can be integrated as a MEVPP.

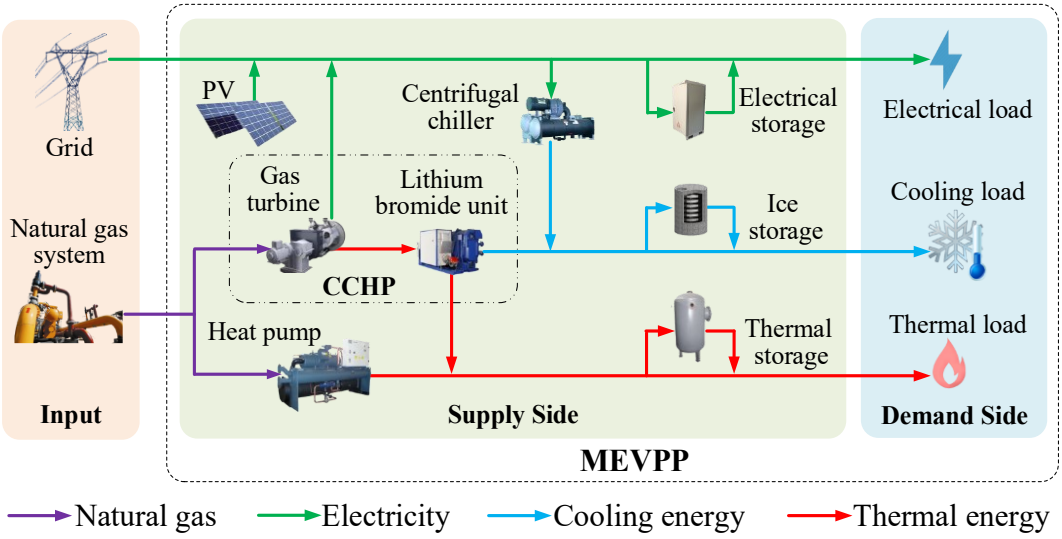

Fig. 2. System structure of MEVPP.

3.1 Demand side

IDR includes the demand response of electricity, cooling and thermal energy. The flexible electrical load is mainly transferable load.

$$P_{\text{eload}}^{t} = P_{\text{edu}}^{t} - P_{\text{tr}}^{t} \tag{1}$$

$$\sum_{t=1}^{N_{\text{T}}} P_{\text{tr}}^{t} = 0 \tag{2}$$

$$-P_{\text{tr}}^{\max} \le P_{\text{tr}}^{t} \le P_{\text{tr}}^{\max} \tag{3}$$

where P_{eload}^{t} is the electrical load after optimization; P_{edu}^{t} is the initial electrical load; P_{tr}^{t} is the transferred electrical load.

The flexible thermal load is mainly hot water load. Users have a desired range for the water temperature [26].

$$V_{\text{cwu}}^{t}(T_{\text{hw}}^{\min} - T_{\text{hw}}^{0}) \le H_{\text{hload}}^{t} / (c_{\text{w}}\rho_{\text{w}}) \le V_{\text{cwu}}^{t}(T_{\text{hw}}^{\max} - T_{\text{hw}}^{0}) \tag{4}$$

where c_{w} and ρ_{w} are the specific heat capacity and density of water, respectively; V_{cwu}^{t} is the volume of cold water; T_{hw}^{0} is the initial water temperature; $T_{\text{hw}}^{\min}$ and $T_{\text{hw}}^{\max}$ are the minimum and maximum water temperature expected by users, respectively; H_{hload}^{t} is the thermal load, which is the required thermal energy to set the water temperature.

The flexible cooling load is similar to thermal load. Users have an acceptable range for the indoor temperature [26].

$$(T_{\text{outu}}^{t} - T_{\text{in}}^{\max}) / R \le C_{\text{cload}}^{t} \le (T_{\text{outu}}^{t} - T_{\text{in}}^{\min}) / R \tag{5}$$

where $T_{\text{in}}^{\min}$ and $T_{\text{in}}^{\max}$ are the minimum and maximum indoor temperature expected by users, respectively; T_{outu}^{t} is the outdoor temperature; R is the thermal resistance of the house; C_{cload}^{t} is the cooling load, which is the required cooling energy to set the indoor temperature.

3.2 Supply side

CCHP consists of a gas turbine and a lithium bromide unit. The electrical energy generated by the gas turbine is:

$$P_{\text{GT}}^{t} = \eta_{\text{GT}}^{\text{e}} \cdot Q_{\text{GT}}^{t} \tag{6}$$

$$0 \le P_{\text{GT}}^{t} \le P_{\text{GT}}^{\text{N}} \tag{7}$$

where P_{GT}^{N} and $\eta_{\text{GT}}^{\text{e}}$ are the rated capacity and the conversion efficiency of natural gas to electricity by the gas turbine; Q_{GT}^{t} is the natural gas consumed by the gas turbine.

The lithium bromide unit model is obtained by (8)-(11).

$$H_{\mathrm{LB}}^{t} \le \eta_{\mathrm{LB}}^{\mathrm{h}} \cdot \eta_{\mathrm{GT}}^{\mathrm{h}} \cdot Q_{\mathrm{GT}}^{t} \tag{8}$$

$$C_{\mathrm{LB}}^{t} \le \eta_{\mathrm{LB}}^{\mathrm{c}} \cdot \eta_{\mathrm{GT}}^{\mathrm{h}} \cdot Q_{\mathrm{GT}}^{t} \tag{9}$$

$$0 \le H_{\mathrm{LB}}^{t} \le x_{\mathrm{LB}}^{t} \cdot H_{\mathrm{LB}}^{\mathrm{N}} \tag{10}$$

$$0 \le C_{\mathrm{LB}}^{t} \le \left(1 - x_{\mathrm{LB}}^{t}\right) \cdot C_{\mathrm{LB}}^{\mathrm{N}} \tag{11}$$

where H_{LB}^{t} and C_{LB}^{t} are the thermal and cooling energy generated by the lithium bromide unit, respectively; $\eta_{\mathrm{LB}}^{\mathrm{h}}$ and $\eta_{\mathrm{LB}}^{\mathrm{c}}$ are the conversion efficiency of the waste heat of flue gas to thermal and cooling energy; $\eta_{\mathrm{GT}}^{\mathrm{h}}$ is the conversion efficiency of natural gas to the waste heat of flue gas; $H_{\mathrm{LB}}^{\mathrm{N}}$ and $C_{\mathrm{LB}}^{\mathrm{N}}$ are the rated thermal and cooling output; x_{LB}^{t} is the binary variable.

The thermal energy generated by heat pump is expressed as:

$$H_{\mathrm{HP}}^{t} = COP_{\mathrm{HP}} \cdot Q_{\mathrm{HP}}^{t} \tag{12}$$

$$0 \le H_{\mathrm{HP}}^{t} \le H_{\mathrm{HP}}^{\mathrm{N}} \tag{13}$$

where COP_{HP} and $H_{\mathrm{HP}}^{\mathrm{N}}$ are the coefficient of performance and the rated output of the heat pump, respectively.

The cooling energy generated by the centrifugal chiller is shown in (14).

$$C_{\mathrm{cen}}^{t} = COP_{\mathrm{cen}} \cdot P_{\mathrm{cen}}^{t} \tag{14}$$

$$0 \le C_{\mathrm{cen}}^{t} \le C_{\mathrm{cen}}^{\mathrm{N}} \tag{15}$$

where COP_{cen} and $C_{\mathrm{cen}}^{\mathrm{N}}$ are the coefficient of performance and the rated output of the centrifugal chiller; P_{cen}^{t} is the electricity consumed by the centrifugal chiller.

The model of the energy storage is as follows:

$$S_{l}^{t} = (1-\alpha_{l}) \cdot S_{l}^{t-1} + \eta_{l}^{\mathrm{c}} \cdot P_{l,\mathrm{c}}^{t} - P_{l,\mathrm{d}}^{t} / \eta_{l}^{\mathrm{d}} \tag{16}$$

$$SoC_{l}^{\min} \cdot S_{l}^{\mathrm{N}} \le S_{l}^{t} \le SoC_{l}^{\max} \cdot S_{l}^{\mathrm{N}} \tag{17}$$

$$0 \le P_{l,\mathrm{c}}^{t}, P_{l,\mathrm{d}}^{t} \le P_{l}^{\max} \tag{18}$$

where $l \in \{\mathrm{e}, \mathrm{h}, \mathrm{c}\}$ is the type of energy storage devices, representing electrical, thermal, and ice storage, respectively; S_{l}^{t} is the energy storage level; α_{l} is the energy loss; $P_{l,\mathrm{c}}^{t}$, $P_{l,\mathrm{d}}^{t}$, η_{l}^{c}, and η_{l}^{d} stand for charging and discharging power

and efficiencies; $SoC_l^{\min}$ and $SoC_l^{\max}$ are minimum and maximum state of charge, respectively; S_l^{N} is the rated energy storage capacity; $P_l^{\max}$ is maximum charging and discharging power.

The demand-supply balance constraints of electricity, thermal energy and cooling energy are formulated in (19)-(21).

$$P_{\mathrm{eload}}^t + P_{\mathrm{cen}}^t + P_{\mathrm{e,c}}^t = P_{\mathrm{pvu}}^t + P_{\mathrm{GT}}^t + P_{\mathrm{grid}}^t + P_{\mathrm{e,d}}^t \tag{19}$$

$$H_{\mathrm{hload}}^t + P_{\mathrm{h,c}}^t = H_{\mathrm{LB}}^t + H_{\mathrm{HP}}^t + P_{\mathrm{h,d}}^t \tag{20}$$

$$n_{\mathrm{room}} C_{\mathrm{cload}}^t + P_{\mathrm{c,c}}^t = C_{\mathrm{cen}}^t + C_{\mathrm{LB}}^t + P_{\mathrm{c,d}}^t \tag{21}$$

where P_{pvu}^t is the power output of PV; P_{grid}^t is the electrical power purchased from the power grid; n_{room} is the number of rooms.

3.3 Peak-regulation constraints

$$\begin{cases} x_{\mathrm{p}}^t P_{\mathrm{f,min}}^t \le P_{\mathrm{p}}^t \le x_{\mathrm{p}}^t P_{\mathrm{p}}^{\max}, t \in T_{\mathrm{p}} \\ P_{\mathrm{p}}^t \le \left(P_{\mathrm{base}}^t - P_{\mathrm{grid}}^t \right), t \in T_{\mathrm{p}} \end{cases} \tag{22}$$

$$\begin{cases} x_{\mathrm{v}}^t P_{\mathrm{f,min}}^t \le P_{\mathrm{v}}^t \le x_{\mathrm{v}}^t P_{\mathrm{v}}^{\max}, t \in T_{\mathrm{v}} \\ P_{\mathrm{v}}^t \le \left(P_{\mathrm{grid}}^t - P_{\mathrm{base}}^t \right), t \in T_{\mathrm{v}} \end{cases} \tag{23}$$

where P_{base}^t is baseline power purchased from the grid; $P_{\mathrm{f,min}}^t$ is lower bound of the bidding power; x_{p}^t and x_{v}^t are binary variables; P_{p}^t and P_{v}^t are the bidding power of peak shaving and valley filling; T_{p} and T_{v} are the peak and valley periods; $P_{\mathrm{p}}^{\max}$ and $P_{\mathrm{v}}^{\max}$ are the upper bounds of the bidding power.

3.4 Objective function

The objective function of MEVPP is calculated by:

$$C_{\mathrm{mvpp}} = \sum_{t=1}^{N_{\mathrm{T}}} \left(C_{\mathrm{buy}}^t + C_{\mathrm{DR}}^t + C_{\mathrm{m}}^t - C_{\mathrm{sell}}^t - C_{\mathrm{f}}^t \right) \tag{24}$$

$$C_{\mathrm{buy}}^t = c_{\mathrm{gas}}^t \left(\frac{P_{\mathrm{GT}}^t}{\eta_{\mathrm{GT}}^{\mathrm{e}}} + \frac{H_{\mathrm{HP}}^t}{\eta_{\mathrm{HP}}} \right) / \varsigma_{\mathrm{gas}} + c_{\mathrm{grid}}^t P_{\mathrm{grid}}^t \tag{25}$$

$$C_{\mathrm{m}}^t = \sum_{l \in \{\mathrm{e,\ h,\ c}\}} c_l \left(P_{l,\mathrm{c}}^t + P_{l,\mathrm{d}}^t \right) \tag{26}$$

where C_{buy}^{t} is the energy cost; C_{DR}^{t} is the compensation cost for users to regulate loads; C_{m}^{t} is the operation cost of energy storage; C_{sell}^{t} is the income from selling energy; C_{f}^{t} is the peak-regulation income; ς_{gas} and c_{gas}^{t} are the calorific value and price of natural gas; c_{grid}^{t} is the price of electricity from the grid; c_{l} is the operation cost coefficient of the energy storage.

The cooling and thermal supplies can meet the needs of users for adjusting indoor temperature and hot water temperature. Therefore, the compensation cost of cooling and thermal loads is not considered.

$$C_{\text{DR}}^{t} = c_{\text{tr}}^{t}\left|P_{\text{tr}}^{t}\right| = c_{\text{tr}}^{t}P_{\text{trs}}^{t} \tag{27}$$

$$-P_{\text{trs}}^{t} \le P_{\text{tr}}^{t} \le P_{\text{trs}}^{t} \tag{28}$$

where c_{tr}^{t} is the compensation price to regulate electrical loads; P_{trs}^{t} is the auxiliary variable.

Energy income from selling energy includes three parts, as in (29). It is worth noting that the energy cost of users should not increase.

$$C_{\text{sell}}^{t} = c_{\text{sc}}^{t}C_{\text{cds}}^{t} + c_{\text{sh}}^{t}H_{\text{hds}}^{t} + c_{\text{se}}^{t}P_{\text{ed}}^{t} \tag{29}$$

$$\begin{cases} C_{\text{cds}}^{t} \le C_{\text{cdbase}}^{t};\ C_{\text{cds}}^{t} \le n_{\text{room}}C_{\text{cload}}^{t} \\ H_{\text{hds}}^{t} \le H_{\text{hdbase}}^{t};\ H_{\text{hds}}^{t} \le H_{\text{hload}}^{t} \end{cases} \tag{30}$$

The income of participating in the peak-regulation market includes the income for peak shaving and valley filling.

$$C_{\text{f}}^{t} = \sum_{t\in T_{\text{p}}} c_{\text{p}}^{t}P_{\text{p}}^{t} + \sum_{t\in T_{\text{v}}} c_{\text{v}}^{t}P_{\text{v}}^{t} \tag{31}$$

where c_{p}^{t} and c_{v}^{t} are the prices for peak shaving and valley filling in the peak-regulation market, respectively.

4. Day-ahead robust bidding model

The uncertainty set of PV generation, and the uncertainty sets of electrical, thermal, and cooling loads are given as:

$$\mathbf{U} = \begin{cases} \mathbf{u} = \{u_{\text{ed}}^{t}, u_{\text{cw}}^{t}, u_{\text{out}}^{t}, u_{\text{pv}}^{t}\} \Big| \\ u_{i}^{t} = u_{i}^{0,t} + b_{i}^{+,t}\Delta u_{i}^{\max,t} - b_{i}^{-,t}\Delta u_{i}^{\max,t} \\ b_{i}^{+,t} + b_{i}^{-,t} \le 1;\ \sum_{t=1}^{T}(b_{i}^{+,t} + b_{i}^{-,t}) \le \Gamma_{i} \end{cases} \tag{32}$$

where uncertainty variables u_{ed}^{t}, u_{cw}^{t}, u_{out}^{t} and u_{pv}^{t} are the actual values of the initial electrical load, the volume of cold water, the outdoor temperature and the power output of PV. $u_i^{0,t}$ and $\mathbf{\Delta}u_i^{\max,t}$ are the predicted nominal value and predicted maximum deviation, respectively. $b_i^{+,t}$ and $b_i^{-,t}$ are the binary variables. Uncertainty budget parameter $\mathbf{\Gamma}_i$ is used to regulate the conservative degree of the robust bidding model.

The uncertainty variables are introduced to the day-ahead bidding model of MEVPP.

$$P_{\mathrm{edu}}^{t}-u_{\mathrm{ed}}^{t}=0 \tag{33}$$

$$V_{\mathrm{cwu}}^{t}-u_{\mathrm{cw}}^{t}=0 \tag{34}$$

$$T_{\mathrm{outu}}^{t}-u_{\mathrm{out}}^{t}=0 \tag{35}$$

$$P_{\mathrm{pvu}}^{t}-u_{\mathrm{pv}}^{t}=0 \tag{36}$$

Therefore, the two-stage robust optimization model established in this paper is as follows [27]:

$$\begin{cases}\min\limits_{\mathbf{x}\in\aleph}\ \max\limits_{\mathbf{u}\in\mathbf{U}}\ \min\limits_{\mathbf{y}\in\mathbf{\Phi}} C_{\mathrm{mvpp}} \\ \quad \text{s.t. (32)} \\ \quad\quad \text{s.t. (1)-(23),(28),(30),(33)-(36)}\end{cases} \tag{37}$$

$$\begin{cases}\aleph=\{x_{\mathrm{LB}}^{t},x_{\mathrm{p}}^{t},x_{\mathrm{v}}^{t}\}; \\ \mathbf{\Phi}=\{P_{\mathrm{GT}}^{t},H_{\mathrm{LB}}^{t},C_{\mathrm{LB}}^{t},H_{\mathrm{HP}}^{t},C_{\mathrm{cen}}^{t},P_{\mathrm{cen}}^{t},P_{\mathrm{eload}}^{t},P_{\mathrm{tr}}^{t}, \\ \quad H_{\mathrm{hload}}^{t},C_{\mathrm{cload}}^{t},P_{\mathrm{grid}}^{t},P_{\mathrm{p}}^{t},P_{\mathrm{v}}^{t},P_{\mathrm{trs}}^{t},C_{\mathrm{cds}}^{t},H_{\mathrm{hds}}^{t}, \\ \quad S_{l}^{t},P_{l,\mathrm{c}}^{t},P_{l,\mathrm{d}}^{t},P_{\mathrm{edu}}^{t},V_{\mathrm{cwu}}^{t},T_{\mathrm{outu}}^{t},P_{\mathrm{pvu}}^{t}\}\end{cases} \tag{38}$$

To solve this problem, the inner min-problem is transformed into the dual problem by the duality theory. Then, it is merged with the middle max-problem. However, after substituting (32), the forms ($b_i^{+,t}\pi_i^{t}$ and $b_i^{-,t}\pi_i^{t}$) of multiplying a binary variable by a continuous variable appear, which are not convex. They are replaced by the new variables $z_i^{+,t}$ and $z_i^{-,t}$ with the following additional linear constraints [28]:

$$\begin{cases}-b_i^{+,t}\mathrm{M}\le z_i^{+,t}\le b_i^{+,t}\mathrm{M};\ -b_i^{-,t}\mathrm{M}\le z_i^{-,t}\le b_i^{-,t}\mathrm{M} \\ \pi_i^{t}-(1-b_i^{+,t})\mathrm{M}\le z_i^{+,t}\le \pi_i^{t}+(1-b_i^{+,t})\mathrm{M} \\ \pi_i^{t}-(1-b_i^{-,t})\mathrm{M}\le z_i^{-,t}\le \pi_i^{t}+(1-b_i^{-,t})\mathrm{M}\end{cases} \tag{39}$$

where π_i^{t} are the dual variables of (33)-(36), respectively; M is a given big value.

After that, a slave problem is obtained, which is a mixed integer linear problem. Finally, the column-and-constraint generation (C&CG) algorithm is used to solve this robust problem [27]. The detailed solving process is given in Appendix A.

5. Validation and analysis

5.1 Parameters and data

Table 1
Parameters of flexible loads.

Parameter	Value	Parameter	Value	Parameter	Value
T_{hw}^{base}	70°C	$[T_{hw}^{min}, T_{hw}^{max}]$	[65°C,75°C]	P_{tr}^{max}	800kW
T_{hw}^{0}	15°C	$[T_{in}^{min}, T_{in}^{max}]$	[22°C,26°C]	c_{tr}^{t}	0.1RMB/kWh
R	18°C/kW	T_{in}^{base}	24°C	n_{room}	3000

The uncertainty budget parameter and maximum deviation for PV are 6 and 15%, and that for electrical, cooling and thermal energy data are 12 and 10%, respectively. The natural gas price is 2.92RMB/m^3. The lower bound of bidding capacity is 0.5MW. Other parameters are given in Table 1 to Table 3. The prediction curves of PV and loads are given in Fig. 3.

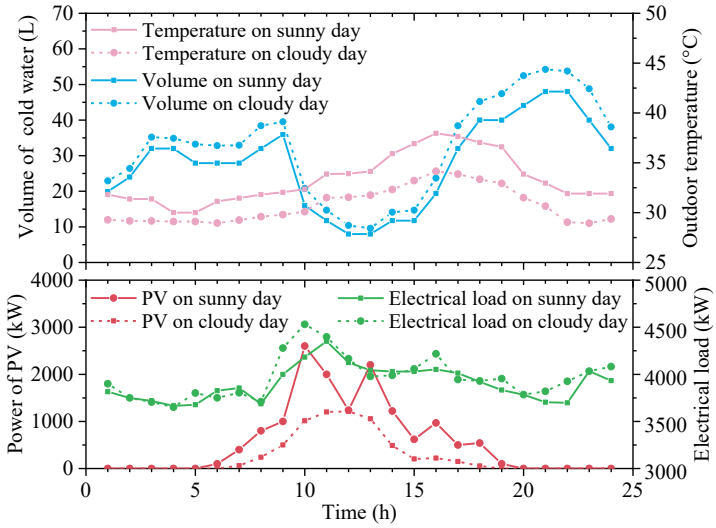

Fig. 3. Prediction curves of PV and loads.

Table 2
Prices of energy and peak-regulation.

Period	Parameter (RMB/kWh)					
	c_{grid}^{t}	c_{p}^{t}	c_{v}^{t}	c_{sc}^{t}	c_{sh}^{t}	c_{se}^{t}
1:00-8:00	0.3249	0	0.35	0.3	0.32	0.7
13:00-17:00; 22:00-24:00	0.6226	0	0			
9:00-12:00; 18:00-21:00	0.9203	0.5	0			

Table 3
Parameters of equipment.

Parameter	Value	Parameter	Value	Parameter	Value	Parameter	Value
η_{LB}^{h} ; η_{LB}^{c}	0.8; 1.2	C_{LB}^{N}	2326kW	c_e	0.02RMB/kWh	η_c^c ; η_c^d	0.95
η_{GT}^{e} ; η_{GT}^{h}	0.35; 0.45	H_{LB}^{N}	2164kW	c_h ; c_c	0.01RMB/kWh	η_e^c ; η_e^d	0.98
COP_{HP} ; COP_{cen}	1.2; 3	C_{cen}^{N}	3000kW	P_{GT}^{N}	2000kW	η_h^c ; η_h^d	0.95
SoC_l^{min} ; SoC_l^{max}	0.1; 0.9	H_{HP}^{N}	2500kW	S_e^N	2000kWh	S_h^N ; S_c^N	1680kWh
P_e^{max} ; P_h^{max}	504kW	α_l	0.01	P_e^{max}	600kW		

5.2 Results and Validation

1) Day-ahead bidding

The robust bidding strategy is used by the MEVPPO to integrate various resources, and the bidding curve is shown in Fig. 4. The valley periods are 1:00-8:00, and peak periods are 9:00-12:00 and 18:00-21:00. The bidding capacity around 11:00 on sunny day is lower than 0.5MW, which does not meet the access condition of the market.

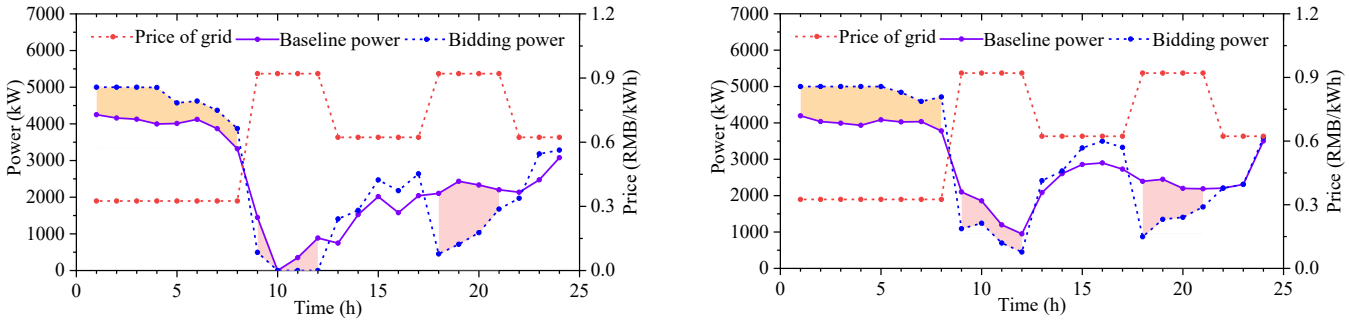

(a) Sunny day (b) Cloudy day

Fig. 4. Day-ahead bidding curve.

2) Day-ahead optimization

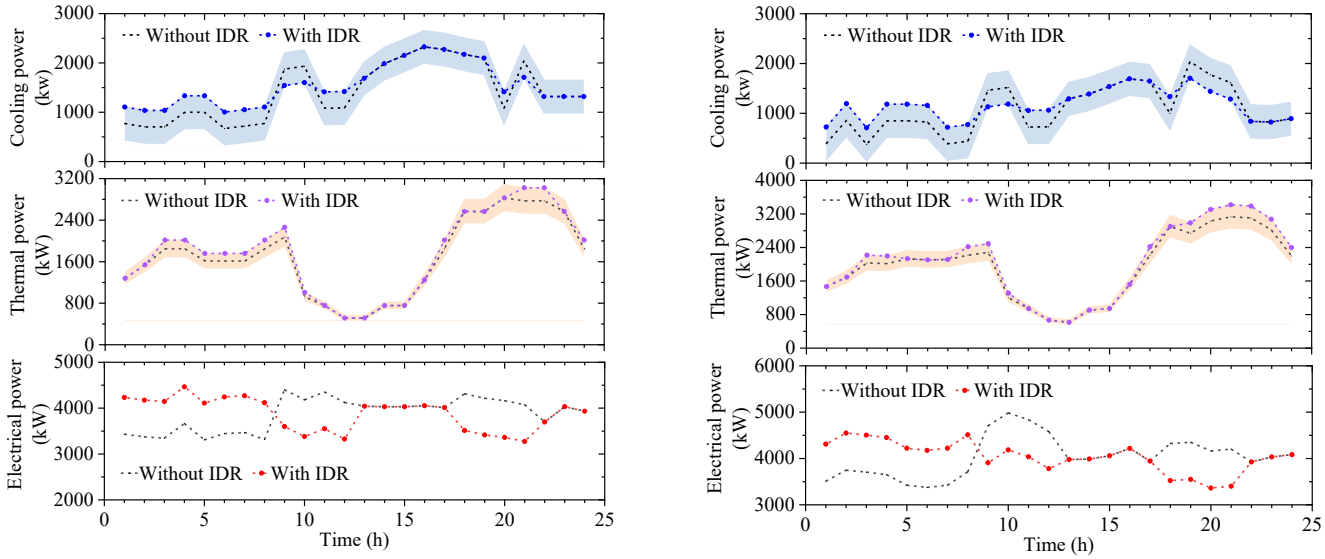

(a) Sunny day (b) Cloudy day

Fig. 5. Load curves without and with IDR.

The load curves without and with IDR are shown in Fig. 5. The shaded areas represent the adjustable range of cooling and thermal loads. Obviously, there are parts of the electrical loads are transferred from peak periods to valley periods, which can reduce electricity cost and increase peak-regulation income. In addition, the cooling demand increases during valley period (1:00-8:00 on sunny and cloudy day) and decreases during peak periods (9:00-10:00 on sunny and cloudy day), which indicates that the variation of cooling load is similar to that of electrical load. The reason is that parts of the cooling energy are generated by the centrifugal chiller consuming electricity. Observe that the thermal demand roughly increases. The thermal load is mainly supplied by the heat pump consuming natural gas, and the price of natural gas is fixed. Thus, to get more income, MEVPP needs to sell more thermal energy.

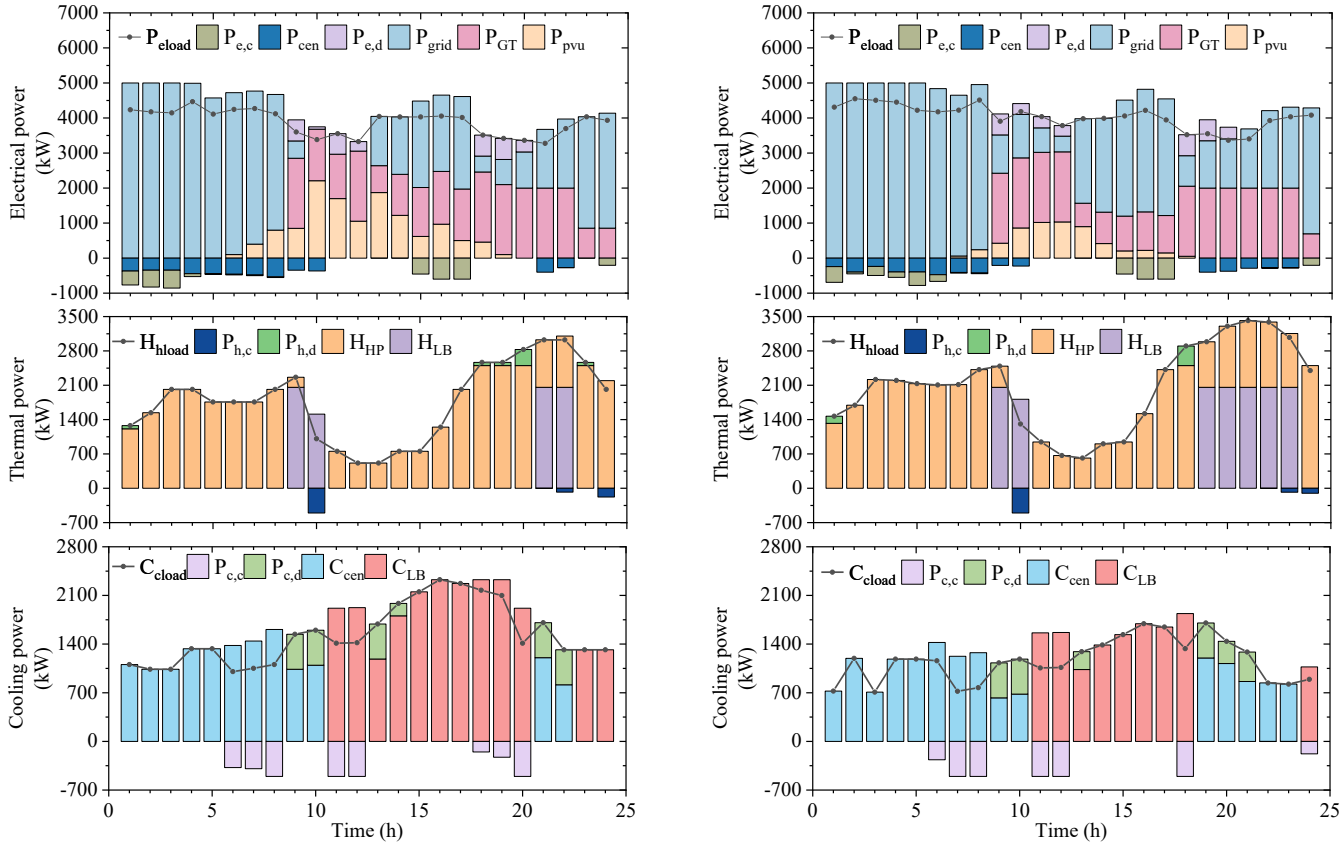

(a) Sunny day (b) Cloudy day

Fig. 6. Output of equipment in supply side.

The day-ahead operation results of equipment in energy supply side are shown in Fig. 6. During valley periods, the electrical storage is charged, and more electricity is purchased from the grid. On the contrary, during peak periods, electrical storage is discharged, and the gas turbine is used to generate electricity, thereby reducing power purchases from the grid. Due to the waste heat generated by the gas turbine during peak hours (9:00-10:00 on sunny and cloudy day; 21:00-22:00 on sunny day and 19-21h on cloudy day), the lithium bromide unit generates thermal energy to

reduce cost. After the thermal demand is met, the remaining thermal energy is stored in the thermal storage (such as 10:00 on sunny and cloudy day) and released at the peak thermal load hours (18:00-20:00 on sunny day and around 18:00 on cloudy day). Cooling supply is similar to thermal supply. It is not discussed because of the limited space.

The optimization results of uncertainties are presented in Fig. 7. The electrical load reduces during valley periods (1:00-3:00 and 5:00-8:00 on sunny day; around 1:00 and 5:00-7:00 on cloudy day) and increases during peak periods (9:00 and 18:00-21:00 on sunny day; 9:00-12:00 and 18:00-21:00 on cloudy day). PV output reduce during peak periods. The cooling load is corresponding to the outdoor temperature, which reduces during valley periods (1:00-3:00 and 6:00-8:00 on sunny day; around1:00, 3:00 and 7:00-8:00 on cloudy day) and increases during peak periods (9:00-10:00 and around 21:00 on sunny day; 9:00-10:00 and 19:00-21:00 on cloudy day). The thermal load is corresponding to the volume of cold water, which decreases during valley periods. In other words, load demand decreases during valley periods and increases during peak periods, but PV output reduces during peak periods. It shows that the peak-regulation capacity gets less. It corresponds to the basic philosophy of robust optimization, which aims to find the worst case within the uncertainty set.

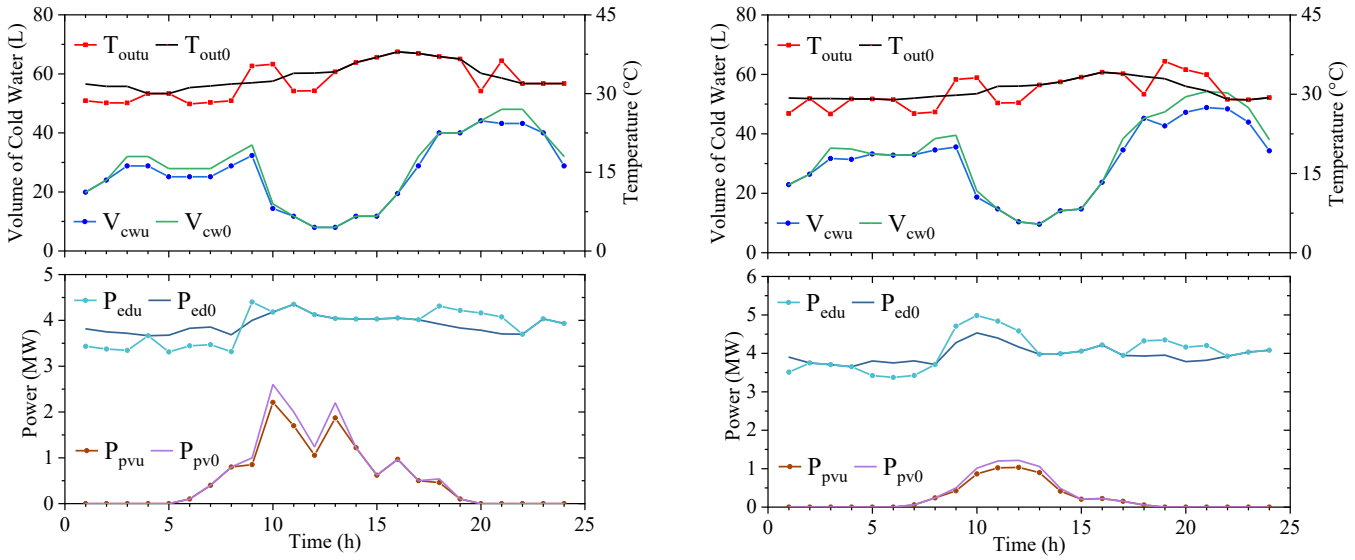

(a) Sunny day

(b) Cloudy day

Fig. 7. Uncertainty optimization results.

3) Demand-side resources

Day-ahead economic analysis of demand-side resource without considering uncertainties is given in Table 4. In Case 1, without IDR and ESSs, MEVPP failed to participate in the peak-regulation market, and the total revenue is the least. Compared with Case 2 and 3, although more load compensation and energy storage costs are spent, the

highest peak-regulation income is obtained in Case 4 with both IDR and ESSs. Moreover, by coordinating IDR and ESSs, the energy cost can be reduced, and ultimately the day-ahead total revenue can be increased.

Table 4
Day-ahead economic analysis of demand-side resource (RMB/day).

Weather	Case	Description		Natural Gas Cost	Electricity Cost	Load Compensation	Storage Cost	Energy Sales Income	Peak-regulation Income	Day-ahead Total Revenue
		IDR	ESSs							
Sunny	1	×	×	30567	30876	0	0	90566	0	29123
	2	✓	×	30626	26873	1270	0	90302	5892	37425
	3	×	✓	31179	28360	0	202	90566	3208	34034
	4	✓	✓	29810	26117	1277	177	90466	7507	40592
Cloudy	1	×	×	30560	37732	0	0	90762	0	22470
	2	✓	×	30895	33353	1280	0	90262	6162	30896
	3	×	✓	30941	35587	0	200	90762	2852	26885
	4	✓	✓	31514	30871	1280	208	90350	8568	35046

4) Trading results

Table 5
Robust optimization performance analysis.

Predicted Deviation		Robust Optimization (RMB/day)						Deterministic Optimization (RMB/day)					
		Day-ahead bidding		Actual operation				Day-ahead bidding		Actual operation			
		Total revenue	Peak-regulation income	Other income	Peak-regulation income	Penalty	Total revenue	Total revenue	Peak-regulation income	Other income	Peak-regulation income	Penalty	Total revenue
Sunny	0%	35398	5465	33288	5465	0	38753	40592	7507	33288	7507	0	40795
	5%			33190	5465	0	38655			33190	7250	0	40440
	10%			32343	5465	0	37809			32343	5993	759	37577
	20%			31030	4541	372	35199			31030	4265	1825	33471
	30%			28447	4363	882	31928			28447	3881	2888	29441
Cloudy	0%	29567	5744	26684	5744	0	32428	35046	8568	26684	8568	0	35252
	5%			26440	5744	0	32185			26440	7846	216	34070
	10%			26362	5744	0	32106			26362	5982	1313	31031
	20%			25894	5239	272	30861			25894	5123	2516	28502
	30%			22230	3979	1318	24891			22230	4018	4670	21578

The actual transaction results are shown in Table 5. Assume that the goal of the actual operation stage is the same as that of the day-ahead operation stage. However, the peak-regulation income and penalty should be calculated based on the actual operation results. Within the predicted deviation range, a group of data is randomly selected as the actual values of uncertainty variables. The peak-regulation penalty price is twice the peak-regulation compensation price. Sunny day is similar to cloudy day. When the predicted deviation is very small (0% and 5%), the actual total revenue of robust optimization is less than deterministic optimization. The reason is that robust optimization has the conservative degree. Its day-ahead bidding capacity is smaller than deterministic optimization, and its peak-regulation income reduces. But when deviation increases, its peak-regulation penalty is less than deterministic optimization so that its actual total revenue is more than deterministic optimization. To conclude, because of the conservative degree of the robust optimization, its day-ahead bidding capacity is smaller, and its day-ahead total revenue reduces. However, in actual operation stage, there is the predicted deviation in PV and loads. Compared with deterministic optimization, the robust optimization can get more revenue in the actual operation stage.

5) Model convergence

The C&CG algorithm is applied to solve day-ahead robust bidding model, and the model convergence result is shown in Fig. 8. It takes 5 iterations on sunny day and 4 iterations on cloudy day to meet the convergence requirements. As the number of iterations increases, the lower bound rises at first and then remains unchanged, which is the characteristics of C&CG algorithm.

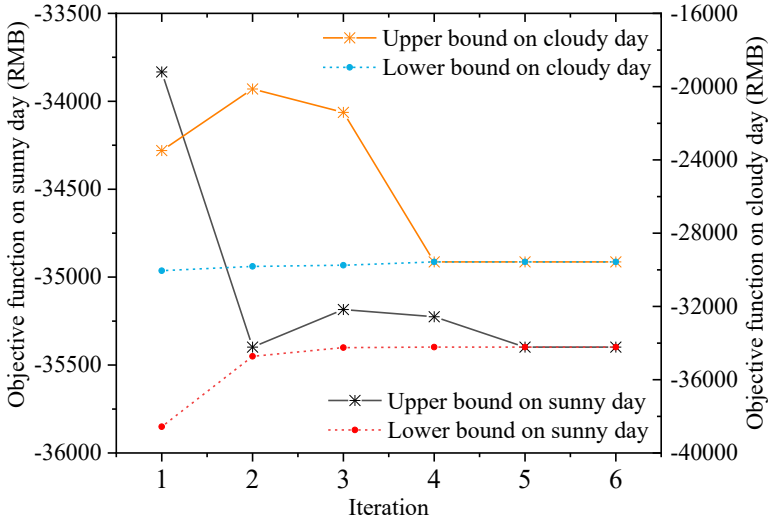

Fig. 8. Model convergence curve based on C&CG algorithm.

6) Conservative degree

The revenue of MEVPP with different uncertainty budget parameters $\boldsymbol{\Gamma}$ are shown in Fig. 9. In the day-ahead bidding stage, with the increase of $\boldsymbol{\Gamma}$, the revenue decreases. In addition, in the actual operation stage, when the predicted deviation is very small (0% and 5%), the revenue decreases. When the deviation increases to 10% and 20%, the revenue increases at beginning, then decreases, and finally flattens out. When the deviation increases to 30%, the revenue increases at first, and finally flattens out. Clearly, MEVPPO can choose benefit and risk by adjusting $\boldsymbol{\Gamma}$.

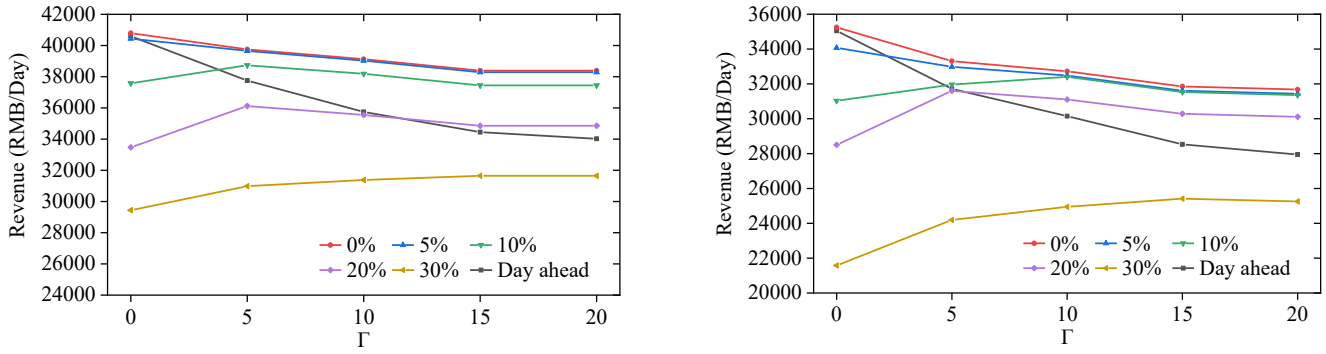

(a) Sunny day (b) Cloudy day

Fig. 9. Revenue with different uncertainty budget parameters.

6. Conclusion

This paper formulates the operation mechanism and a day-ahead robust bidding model for MEVPP in peak-regulation market. Case studies reveal that the mechanism can integrate various resources of electricity, cooling energy, thermal energy, and natural gas in energy demand and supply sides to participate in the peak-regulation market and improve the economy of the system. Compared with Case 1 (without IDR and ESSs), the day-ahead total revenue respectively increased by 39% on sunny day and 56% on cloudy day in Case 4 by utilizing IDR and ESSs at the same time. In addition, compared with deterministic optimization method, the proposed robust optimization method considering multiple uncertainties can resist the risk of PV output and load power fluctuations and reduce the peak-regulation penalty in the actual operation stage.

To further improve the proposed methodology, the investigation on the refined modelling of the devices and loads will be considered in in the future.

Acknowledgement

This work was supported in part by the International Science and Technology Cooperation Program of China under Grant 2022YFE0129300, in part by the National Natural Science Foundation of China under Grant U22B200134, and in part by the Royal Society-Newton Advanced Fellowship under grant NAF\R1\201036.

Appendix A

Algorithm A1

1: Set $v = 0$ and initialize $\mathbf{x}^{(0)}$.

2: Set $\mathrm{UB}_v \to +\infty$ and $\mathrm{LB}_v \to -\infty$.

3: **while** $\mathrm{UB}_v - \mathrm{LB}_v > \varepsilon$ **do**

4: Update $v = v + 1$.

5: Solve the slave problem (A4) for given $\mathbf{x}^{(v-1)}$.

6: Get $\mathbf{u}^{(v)}$ and update UB_v using (A5).

7: Solve the master problem (A6) for given $\mathbf{u}^{(k)}(k = 1, \cdots, v)$.

8: Obtain $\mathbf{x}^{(v)}$ and update LB_v using (A7).

9: **end while**

10: Output $\mathbf{x}^{(v)}$, $\mathbf{y}^{(v)}$ and $\mathbf{u}^{(v)}$.

The day-ahead two-stage robust bidding model is re-written in the following matrix form:

$$\begin{cases} \min\limits_{\mathbf{x}} \ \max\limits_{\mathbf{u}\in\mathbf{U}} \ \min\limits_{\mathbf{y}} \ \mathbf{c}^{\mathrm{T}}\mathbf{y} \\ \quad\quad\quad\quad \text{s.t. } \mathbf{E}\mathbf{y} + \mathbf{F}\mathbf{x} \geq \mathbf{d} : \boldsymbol{\lambda} \\ \quad\quad\quad\quad\quad\ \mathbf{K}\mathbf{y} = \mathbf{0} \quad\ : \boldsymbol{\nu} \\ \quad\quad\quad\quad\quad\ \mathbf{I}_u\mathbf{y} = \mathbf{u} \quad\ : \boldsymbol{\pi} \end{cases} \tag{A1}$$

where $\mathbf{x}$ is the binary variable in the first stage; $\mathbf{u}$ and $\mathbf{y}$ are the uncertainty variable and the continuous variable in the second stage, respectively; $\mathbf{c}$ is the coefficient column vector corresponding to the objective function; $\mathbf{E}$, $\mathbf{F}$, $\mathbf{K}$, $\mathbf{I}_u$ and $\mathbf{d}$ are the coefficient matrix and constant column vector of the corresponding constraints, respectively; $\boldsymbol{\lambda}$, $\boldsymbol{\nu}$ and $\boldsymbol{\pi}$ are the dual variables.

The uncertainty set is as following:

$$\mathbf{U} = \begin{cases} u_i^t = u_i^{0,t} + b_i^{+,t}\Delta u_i^{\max,t} - b_i^{-,t}\Delta u_i^{\max,t} \\ b_i^{+,t} + b_i^{-,t} \leq 1;\ \sum\limits_{t=1}^{T}(b_i^{+,t} + b_i^{-,t}) \leq \boldsymbol{\Gamma}_i \end{cases} \tag{A2}$$

The C&CG algorithm is used to solve the robust problem by transforming the initial two-stage robust problem into a master problem and a slave problem. Firstly, the inner min-problem is transformed into the dual problem by the duality theory. Then, it is merged with the middle max-problem.

$$\begin{cases} \max\limits_{\mathbf{u},\boldsymbol{\lambda},\boldsymbol{\nu},\boldsymbol{\pi}} \ (\mathbf{d} - \mathbf{F}\mathbf{x})^{\mathrm{T}}\boldsymbol{\lambda} + \mathbf{u}^{\mathrm{T}}\boldsymbol{\pi} \\ \text{s.t. } \ \mathbf{E}^{\mathrm{T}}\boldsymbol{\lambda} + \mathbf{K}^{\mathrm{T}}\boldsymbol{\nu} + \mathbf{I}_u{}^{\mathrm{T}}\boldsymbol{\pi} = \mathbf{c} \\ \quad\quad \boldsymbol{\lambda} \geq \mathbf{0};\ \boldsymbol{\nu}, \boldsymbol{\pi} : \textit{free} \\ \quad\quad \mathbf{u} \in \mathbf{U} \end{cases} \tag{A3}$$

However, after substituting Equation (A2) to (A3), the forms of multiplying the binary variable by the continuous variable appear, which are not convex. In this paper, they are linearized. And then the slave problem is formed.

$$\max_{\mathbf{z}^+,\mathbf{z}^-,\mathbf{b}^+,\mathbf{b}^-,\boldsymbol{\lambda},\mathbf{v},\boldsymbol{\pi}} (\mathbf{d}-\mathbf{F}\mathbf{x}^{(v-1)})^{\mathrm{T}}\boldsymbol{\lambda}+(\mathbf{u}^0)^{\mathrm{T}}\boldsymbol{\pi}+(\Delta\mathbf{u}^{\max})^{\mathrm{T}}\mathbf{z}^+-(\Delta\mathbf{u}^{\max})^{\mathrm{T}}\mathbf{z}^-$$

$$\text{s.t.}\begin{cases}\mathbf{E}^{\mathrm{T}}\boldsymbol{\lambda}+\mathbf{K}^{\mathrm{T}}\mathbf{v}+\mathbf{I}_u{}^{\mathrm{T}}\boldsymbol{\pi}=\mathbf{c}\\ \boldsymbol{\lambda}\geq\mathbf{0};\ \mathbf{v},\boldsymbol{\pi}:\textit{free}\\ -\mathbf{b}^+\mathrm{M}\leq\mathbf{z}^+\leq\mathbf{b}^+\mathrm{M};\ -\mathbf{b}^-\mathrm{M}\leq\mathbf{z}^-\leq\mathbf{b}^-\mathrm{M}\\ \boldsymbol{\pi}-(\mathbf{1}-\mathbf{b}^+)\mathrm{M}\leq\mathbf{z}^+\leq\boldsymbol{\pi}+(\mathbf{1}-\mathbf{b}^+)\mathrm{M}\\ \boldsymbol{\pi}-(\mathbf{1}-\mathbf{b}^-)\mathrm{M}\leq\mathbf{z}^-\leq\boldsymbol{\pi}+(\mathbf{1}-\mathbf{b}^-)\mathrm{M}\\ \mathbf{b}^++\mathbf{b}^-\leq\mathbf{1};\ \sum_{t=1}^{T}(\mathbf{b}^++\mathbf{b}^-)\leq\boldsymbol{\Gamma}\end{cases}\tag{A4}$$

where $\mathbf{x}^{(v-1)}$ is the known value, which is optimized in the master problem; $\mathbf{z}^+$ and $\mathbf{z}^-$ are the auxiliary variables; M is a given big value.

Thus, $\mathbf{u}^{(v)}$ and the upper bound can be obtained:

$$\mathrm{UB}_v=(\mathbf{d}-\mathbf{F}\mathbf{x}^{(v-1)})^{\mathrm{T}}\boldsymbol{\lambda}^{(v)}+(\mathbf{u}^0)^{\mathrm{T}}\boldsymbol{\pi}^{(v)}+(\Delta\mathbf{u}^{\max})^{\mathrm{T}}(\mathbf{z}^+)^{(v)}-(\Delta\mathbf{u}^{\max})^{\mathrm{T}}(\mathbf{z}^-)^{(v)}\tag{A5}$$

In addition, the master problem is obtained by decomposing (A1):

$$\begin{cases}\min\limits_{\mathbf{x},\eta,\mathbf{y}^{(k)},k=1,\cdots,v}\ \eta\\ \text{s.t.}\ \ \eta\geq\mathbf{c}^{\mathrm{T}}\mathbf{y}^{(k)};\ \mathbf{E}\mathbf{y}^{(k)}+\mathbf{F}\mathbf{x}\geq\mathbf{d},\\ \qquad\mathbf{K}\mathbf{y}^{(k)}=\mathbf{0};\ \ \mathbf{I}_u\mathbf{y}^{(k)}=\mathbf{u}^{(k)}\end{cases}\tag{A6}$$

where $\mathbf{u}^{(k)}(k=1,\cdots,v)$ is the known value, which is optimized in the slave problem.

Thus, $\mathbf{x}^{(v)}$ and the lower bound can be obtained:

$$\mathrm{LB}_v=\eta^{(v)}\tag{A7}$$

Finally, the C&CG method is used to solve the master problem and slave problem, respectively. The process of C&CG algorithm is shown in Algorithm A1.

References

[1] D. Yang, S. He, Q. Chen, D. Li, and H. Pandžić, "Bidding strategy of a virtual power plant considering carbon-electricity trading," *CSEE Journal of Power and Energy Systems,* vol. 5, no. 3, pp. 306-314, Sep. 2019.

[2] S. Zhang, X. Kong, Y. Shen, W. Hu and T. Ma, " Optimal Economic Dispatch of Virtual Power Plant based on Bidding," in *2020 23rd International Conference on Electrical Machines and Systems (ICEMS)*, Hamamatsu, Japan, 2020, pp. 467-471.

[3] S. Yin, Q. Ai, J. Li, Z. Li, and S. Fan, "Energy Pricing and Sharing Strategy Based on Hybrid Stochastic Robust Game Approach for a Virtual Energy Station With Energy Cells," *IEEE Transactions on Sustainable Energy,* vol. 12, no. 2, pp. 772-784, Apr. 2021.

[4] H. Zhao, J. Chen, B. Wang, X. Shang, J. Zhuang, and H. Sun, "A Robust Aggregate Model for Multi-Energy Virtual Power Plant in Grid Dispatch," in *2019 IEEE Sustainable Power and Energy Conference (iSPEC)*, Beijing, China, 2019, pp. 1631-1636.

[5] X. Jin, J. Wang, X. Shen, H. Wang, and R. Liu, "An Overview of Virtual Power Plant Development from the Perspective of Market Participation," in *2018 2nd IEEE Conference on Energy Internet and Energy System Integration (EI2)*, Beijing, China, 2018, pp. 1-6.

[6] J. Wang, X. Shen, Y. Xu, Q. Guo, H. Sun, and Y. Chen, "Ancillary service for frequency regulation based on multi-energy virtual power plant aggregating factory load," in *The 11th IET International Conference on Advances in Power System Control, Operation and Management (APSCOM 2018)*, Hong Kong, China, 2018, pp. 1-7.

[7] Z. Luo, S. Hong, and Y. Ding, "A data mining-driven incentive-based demand response scheme for a virtual power plant," *Applied Energy,* vol. 239, pp. 549-559, Apr. 2019.

[8] L. Ju, R. Zhao, Q. Tan, Y. Lu, Q. Tan, and W. Wang, "A multi-objective robust scheduling model and solution algorithm for a novel virtual power plant connected with power-to-gas and gas storage tank considering uncertainty and demand response," *Applied Energy,* vol. 250, pp. 1336-1355, Sep. 2019.

[9] L. Dong, S. Fan, Z. Wang, J. Xiao, H. Zhou, Z. Li, and G. He, "An adaptive decentralized economic dispatch method for virtual power plant," *Applied Energy*, vol. 300, p. 117347, Oct. 2021.

[10] S. Hadayeghparast, A. SoltaniNejad Farsangi, and H. Shayanfar, "Day-ahead stochastic multi-objective economic/emission operational scheduling of a large scale virtual power plant," *Energy*, vol. 172, pp. 630-646, Apr. 2019.

[11] T. M. Alabi, L. Lu, and Z. Yang, "Improved hybrid inexact optimal scheduling of virtual powerplant (VPP) for zero-carbon multi-energy system (ZCMES) incorporating Electric Vehicle (EV) multi-flexible approach," *Journal of Cleaner Production*, vol. 326, p. 129294, Dec. 2021.

[12] National Energy Administration, Work Plan for Improving the Compensation (Market) Mechanism for Auxiliary Power Services, Beijing, China, 2017.

[13] National Energy Administration, 14th Five-Year Plan for Modern Energy System, Beijing, China, 2022.

[14] L. Ya, Z. Deliang, and W. Xuanyuan, "A Peak Regulation Ancillary Service Optimal Dispatch Method of Virtual Power Plant Based on Reinforcement Learning," in *2019 IEEE Innovative Smart Grid Technologies - Asia (ISGT Asia)*, Chengdu, China, 2019, pp. 4356-4361.

[15] P. Li, J. Yang, and J. Liu, "Distributed Cooperative Clearing Model of Peak Regulation Ancillary Service Market Under Ubiquitous Power Internet of Things," in *2021 International Conference on Power System Technology (POWERCON)*, Haikou, China, 2021, pp. 690-695.

[16] J. Zhao, B. Cong, Y. Yang, H. Ye, X. Ling, and X. Wang, "Two Stage Deep Peak Regulation Ancillary Service Market Clearing Model Considering Virtual Power Plant," in *2021 IEEE 5th Conference on Energy Internet and Energy System Integration (EI2)*, Taiyuan, China, 2021, pp. 3534-3538.

[17] Y. Wang, Z. Shi, Z. Wang, J. Wang, X. Li, Y. Zheng, P. Wang, Y. Hu, and J. Deng, "Dynamic scheduling optimization model for virtual power plant connecting with wind-photovoltaic-energy storage system," in *2017 IEEE Conference on Energy Internet and Energy System Integration (EI2)*, Beijing, China, 2017, pp. 1-6.

[18] S. R. Dabbagh and M. K. Sheikh-El-Eslami, "Risk Assessment of Virtual Power Plants Offering in Energy and Reserve Markets," *IEEE Transactions on Power Systems,* vol. 31, no. 5, pp. 3572-3582, Sep. 2016.

[19] J. Shen, C. Jiang, Y. Liu, and X. Wang, "A Microgrid Energy Management System and Risk Management Under an Electricity Market Environment," *IEEE Access,* vol. 4, pp. 2349-2356, Apr. 2016.

[20] D. Zhang, Z. Hu, and X. Wang, "A Risk-Constrained Model for Virtual Power Plants Including DGs and Coupled Electricity-Heat Supply," in *2019 IEEE 8th International Conference on Advanced Power System Automation and Protection (APAP)*, Xi'an, China, 2019, pp. 830-834.

[21] C. Wang, Y. Zhou, J. Wu, J. Wang, Y. Zhang, and D. Wang, "Robust-Index Method for Household Load Scheduling Considering Uncertainties of Customer Behavior," *IEEE Transactions on Smart Grid,* vol. 6, no. 4, pp. 1806-1818, Jul. 2015.

[22] C. J. M. Sampang, P. I. S. D. Ibarbia, C. T. Laxamana, and A. C. Nerves, "Optimal Scheduling Strategy for Virtual Power Plants with Interruptible Loads," in *2018 IEEE PES Asia-Pacific Power and Energy Engineering Conference (APPEEC)*, Kota Kinabalu, Malaysia, 2018, pp. 616-620.

[23] X. Guo, C. Cai, H. Shi, Y. Xie, and Y. Zhang, "Robust based optimal operation model of virtual power plant in electricity market," in *2021 China International Conference on Electricity Distribution (CICED)*, Shanghai, China, 2021, pp. 1015-1019.

[24] W. Tang and H. Yang, "Optimal Operation and Bidding Strategy of a Virtual Power Plant Integrated With Energy Storage Systems and Elasticity Demand Response," *IEEE Access,* vol. 7, pp. 79798-79809, Jun. 2019.

[25] M. Rahimiyan and L. Baringo, "Strategic Bidding for a Virtual Power Plant in the Day-Ahead and Real-Time Markets: A Price-Taker Robust Optimization Approach," *IEEE Transactions on Power Systems,* vol. 31, no. 4, pp. 2676-2687, Jul. 2016.

[26] F. Brahman, M. Honarmand, and S. Jadid, "Optimal electrical and thermal energy management of a residential energy hub, integrating demand response and energy storage system," *Energy and Buildings,* vol. 90, pp. 65-75, Mar. 2015.

[27] B. Zeng and L. Zhao, "Solving two-stage robust optimization problems using a column-and-constraint generation method," *Operations Research Letters,* vol. 41, no. 5, pp. 457-461, Sep. 2013.

[28] Y. Tan, Y. Li, Y. Cao, and M. Shahidehpour, "Integrated Optimization of Network Topology and DG Outputs for MVDC Distribution Systems," *IEEE Transactions on Power Systems,* vol. 33, no. 1, pp. 1121-1123, Jan. 2018.